Supporting Information
for

Transistor Configuration Yields Energy Level Control in Protein-Based Junctions

Ben Kayser[1], Jerry A. Fereiro[1], Cunlan Guo[2,#], Sidney Cohen[3], Mordechai Sheves[2*], Israel Pecht[4*], David Cahen[1*]

[1]Department of Materials and Interfaces, Weizmann Institute of Science, Rehovot, 76100.
[2]Department of Organic Chemistry, Weizmann Institute of Science, Rehovot, 76100.
[3]Department of Chemical Research Support, Weizmann Institute of Science, Rehovot, 76100.
[4]Department of Immunology, Weizmann Institute of Science, Rehovot, 76100.
[#] Present address: Key Laboratory of Analytical Chemistry for Biology and Medicine, College of Chemistry and Molecular Sciences, Wuhan University, Wuhan, P. R. China, 430072
*mudi.sheves@weizmann.ac.il; israel.pecht@weizmann.ac.il; david.cahen@weizmann.ac.il

Contents:

SI-1) Device Fabrication

Initially, to further improve gate-coupling (defined as the energy level shift resulting from the applied gate voltage) to the junction and inhibit electrical shorting, the SiO_2 between the electrodes was dry-etched (ICP) by 100 nm (with CF_4 and O_2 at 10 V and 300 W for 90 s), using the gold-patterned device as a mask for vertical etching with a high aspect ratio. These ICP parameters are optimal for preserving the topography of the gold surface, crucial for routine protein binding procedures. A scheme of the device, made in this way, is shown in figure 1 of the main text. This step was eliminated at a later stage because debris were found to be deposited on the sample during the ICP step.

Optimization of the parameters described above, then allowed use of samples without this step, albeit with lower junction yield, and hence we report here results obtained with both types of samples. Scanning electron microscopy (SEM, Fig. 1b and 1c) and AFM (see SI2 and SI3 below) were used to characterize the topography.

The figure below shows ellipsometry data of SiO_2 thickness as function of etching yime using the ICP parameters outlined above. Thus, for a 1.5 minute etch time ~ 100 nm of oxide was removed.

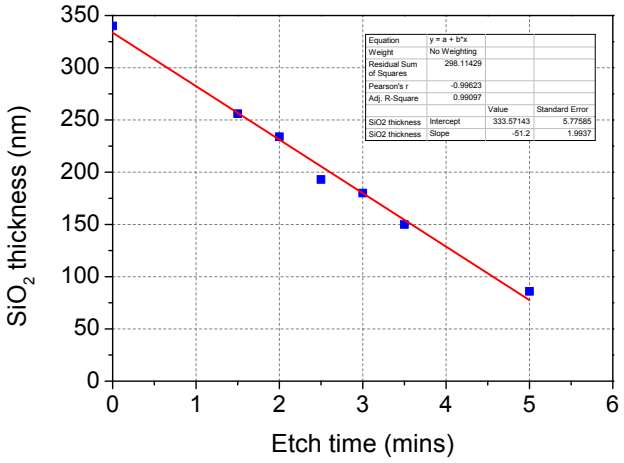

After protein immobilization (detailed in the experimental section of the main text) the device is wedge-bonded to a designed printed circuit board (PCB) using a 25 µm diameter gold wire. The four junctions are soldered from the PCB to external wires so as to allow for plug-and-play as seen in the image below:

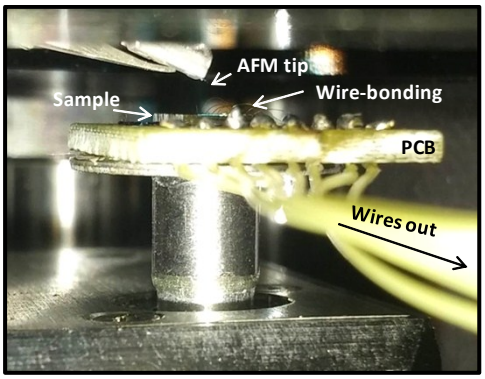

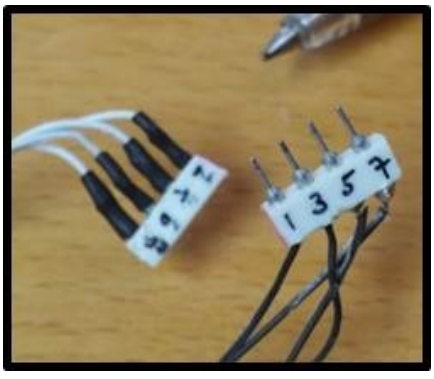

Left) Internal AFM set-up, showing the sample mounted on a magnetic stub, ready for measurement. **Right**) Drain (male connectors) and gate (female connectors) electrodes that allow for easy interchange between junctions.

Below are shown the AFM topography images of the height difference between interdigitated gate and drain arms after EBL patterning, deposition of metals by

evaporation and subsequent lift-off: a) AFM topography image of drain (upper) and gate (lower) arms; b) height cross section of (vertical) line shown in the left image; c) 3D representation of raised gate and drain rotated 180º from the middle image

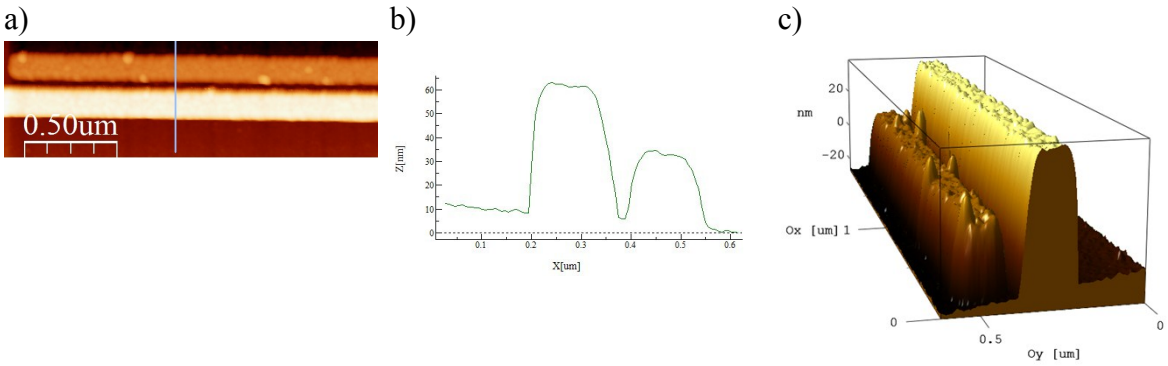

SI-2) UV-visible spectra of holo- and apo-Azurin solutions. The 625 nm absorption band is due to ligand to the Cu(II) charge transfer in holo-Azurin. This band disappears upon Cu(II) removal. Both variants contain a signature tryptophan shoulder at 292 nm.

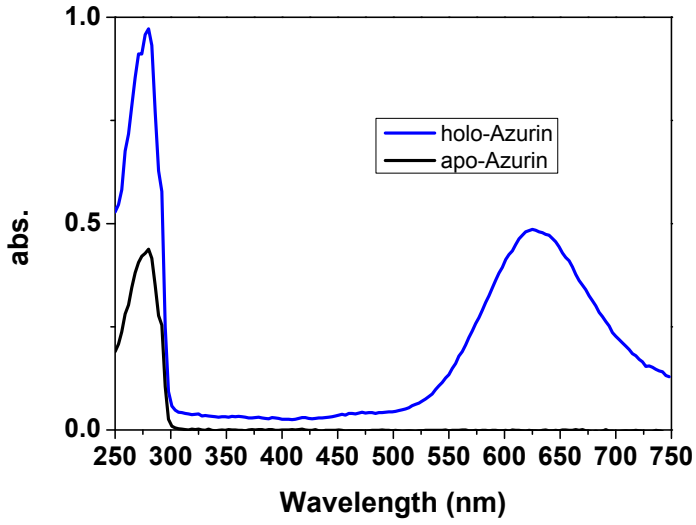

SI-3) AFM topography scans. The monolayer thicknesses of holo- and apo-Azurin were both consistently 2 nm (as measured by ellipsometry):

A) Bare gold (~0.9 nm roughness)

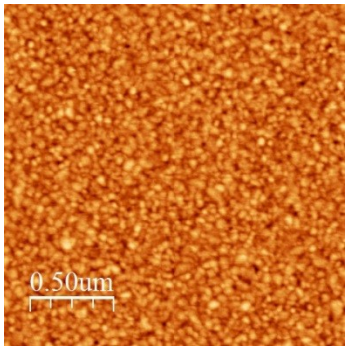

B) Holo-Azurin monolayer on gold

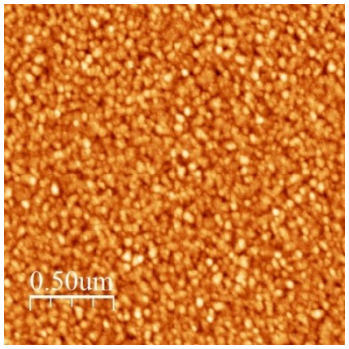

C) Apo-Azurin monolayer on gold

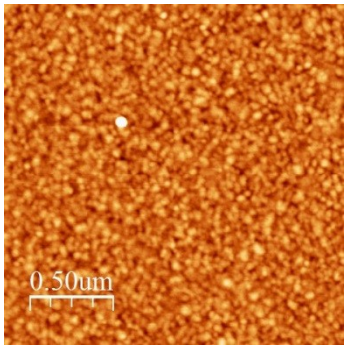

SI-4) Left) AFM scratch (100 nN) of apo-Azurin monolayer and subsequent topography scan, performed to confirm depth of the well and, hence, the monolayer thickness, which is found to be ~2 nm. This value is based on its crystallographic structure and is consistent with previous work and corresponds to a tilted orientation of the bound protein, **Right**) Height cross-section across the center of the square well in the AFM figure on the left; the depth of the well, and hence, thickness of the monolayer is ~ 2 nm.

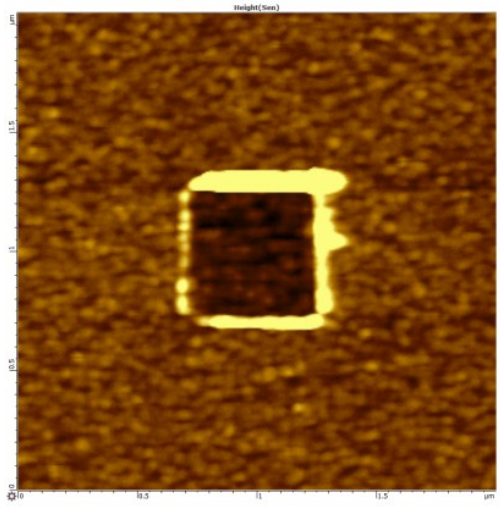

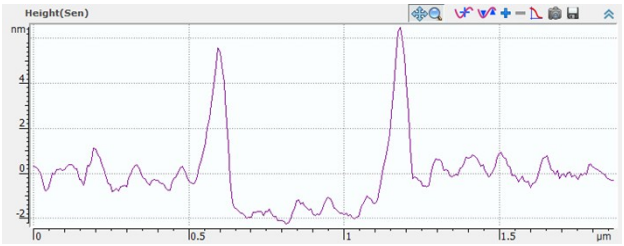

SI-5) Polarization modulation-infrared reflection-adsorption spectra (PM-IRRAS) of holo- and apo-Azurin monolayers on gold. Relative positions and ratios of amide I and II absorption peaks are the same, indicating that the conformation of Azurin in both monolayers is the same.

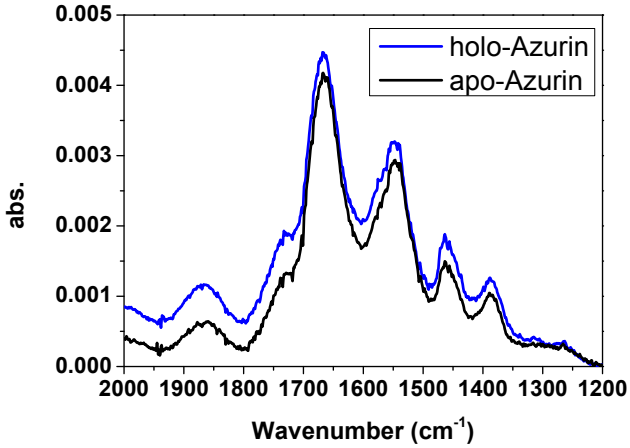

SI-6) Examples of gate leakage: Devices that exhibited electrical shorting behaviour (i.e. nA currents or spiking) through the gate leakage were not further studied and their characteristics were not included in averaging statistics:
a) Breakdown through the ~ 80 nm drain-gate channel of SiO_2 was sometimes observed in devices, leading to > 10 nA currents at V_G = 20 V (contrast to Fig. 2a,b in main text);
b) Gate sweep showing gate-current spikes (seen in the red-dashed box at ~ 15 V_G) that were sometimes observed (i.e., non-capacitive currents), which are indicative of filling of charge traps in the dielectric or partial shorting across the drain-gate channel; this sometimes led to spurious I_{SD} currents, which can be attributed to a gate artefact.

a) **b)**

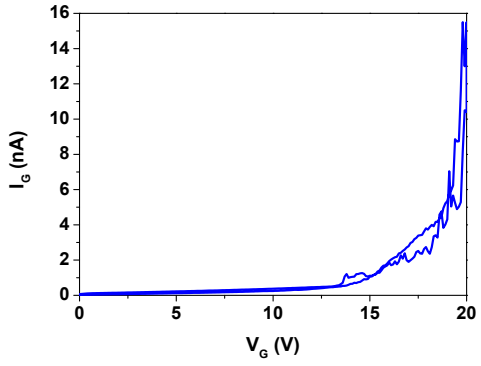

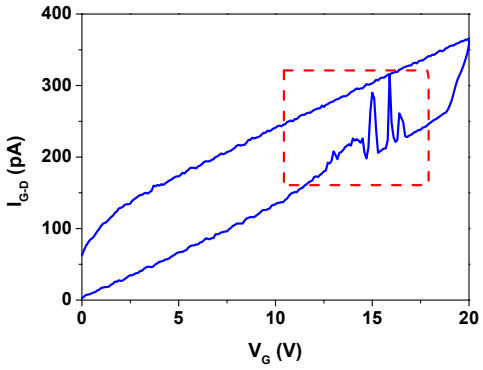

SI-7) Electrical measurements of holo-Azurin in the negative gate bias range. **a**) differential conductance plots, made by differentiating I-V curves, and with negative gate bias (compare to Figs. 3a, b in the main text); b) Gate sweep in the negative V_G range; non-zero current at 10 mV_{SD} shows that good contact is maintained during the sweep, but that no current onset is seen, in comparison with positive V_G (as shown in figs. 2a, 4b and 4c in main text).

a)

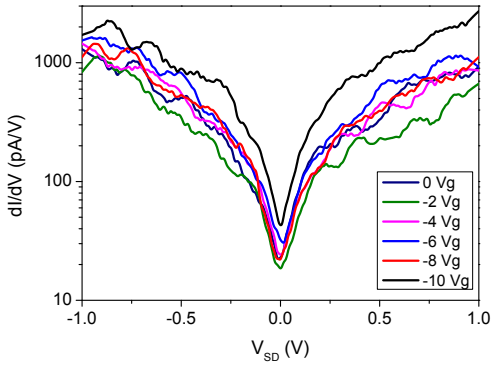

b)

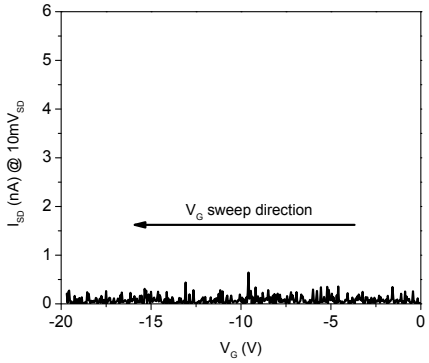

SI-8a) Gate sweep of apo-Azurin junction at 10 mV_{SD}. The arrows and numbers indicate the direction and order in which this sweep was carried out. The rise of 20 pA in the positive gate range is not significant given that, for apo-Azurin (as stated in the main text and fig. 2b), the currents don't rise above a few tens of pA across the whole V_G range. Due to the measurement dwelling time constraints mentioned in the paper it was not possible to sweep between +20 to -20 V_G in one measurement.

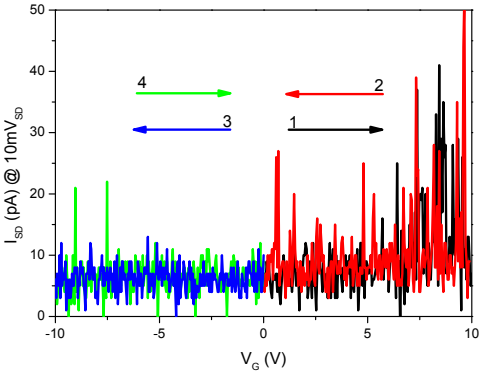

SI-8b) The first two graphs below are cropped from figures 2A and 4B of the main text (for holo-Azurin), representing

i) Pt-Azurin-Au and,

ii) Au-Azurin-Au configurations.

They show the source-drain currents (I_{SD}) only between 0 – 5 V_G in order to illustrate the low currents at ~ 0 V_G. Comparing currents in i) with ii), we observe that at ~ 0 V_G currents are higher for Au tips than with Pt tips. For clarity, forward and reverse sweeps are offset by 50 pA.

iii) V_G sweep at 10 mV_{SD} for apo-Azurin, cropped from figure 2B in the main text. The currents via apo-Azurin are higher (than via holo-Azurin) although this could represent a broader spread in conductance possibly due to lower mechanical rigidity of apo-Azurin [1], as has been reported in a recent EC-STM study comparing holo- and apo-Azurin [2].

iv) comparison of a typical I-V trace for holo- (black) with that of apo-Azurin (red) at 6 nN Pt tip force, where each trace is an average of 10 I-V's, measured on the same spot.

i)

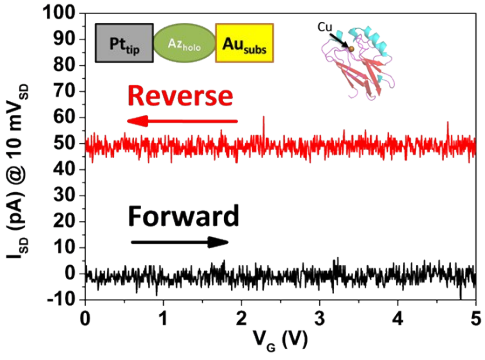

ii)

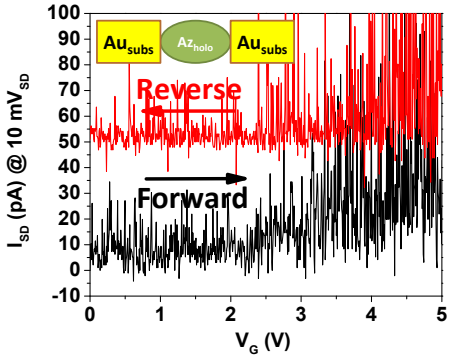

iii)

iv)

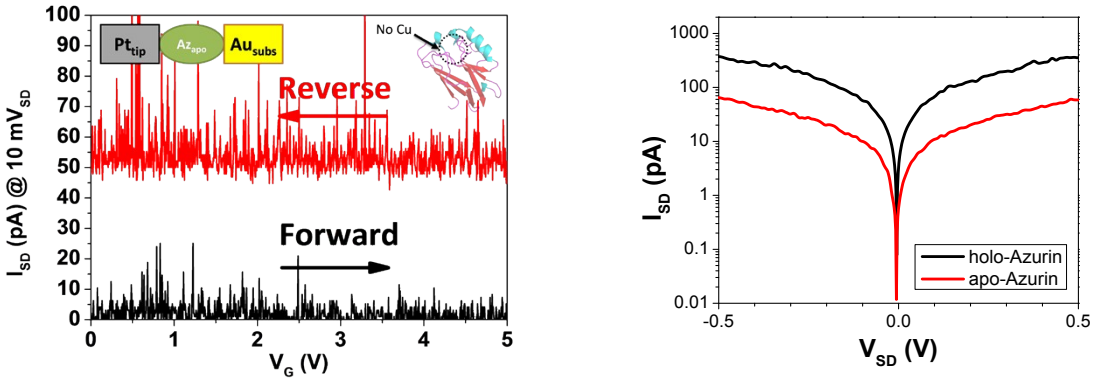

SI-8c) Further V_G sweeps at 10 mV_{SD} for Pt-(holo)Azurin-Au junctions. Plots a) and b) were taken using two separate devices on different days of measuring that show *no gate-induced current onset* (defined as currents that rise above 0.5 nA). A Pt-coated AFM tip is brought into contact with the Azurin monolayer with a force of 4 nN on the drain electrode. After an I-V is measured (with current magnitudes consistent with previous measurements), the tip is then held at 10 mV_{SD} on that same spot and V_G is swept from 0 to 20 V_G ('forward scan', black) then immediately from 20 to 0 V_G ('backwards scan', red). In these graphs the backwards scan is offset by 200 pA for clarity. There is a difference in the noise level between a) and b) despite being measured under the same conditions. This difference could arise from variability of the contact made in each scan i.e. differences in the force feedback between experiments, slight differences in the contact area between tips and differences in the location of the exact contact between the AFM tip on the protein surface. Both graphs are examples of junctions that show no gate-induced current onset, which results from screening of the gate field.

a)

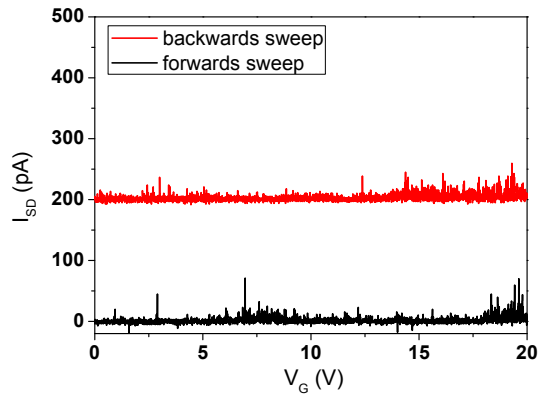

b)

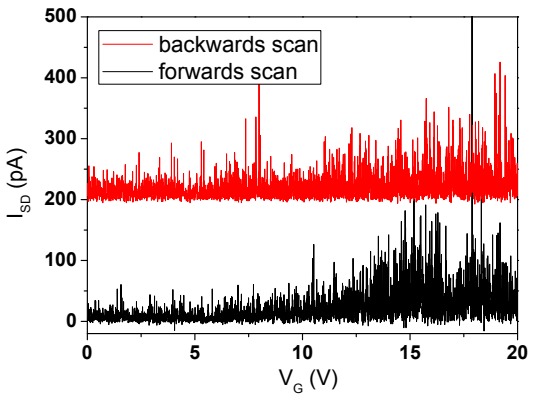

SI-9) AFM topography scan for Pt_{tip}-Azurin-$Au_{electrode}$ (left) and Au_{tip}-Azurin-$Au_{electrode}$ (right) using the same Azurin monolayer in the same measuring session. The root mean squared (RMS) roughness of Azurin monolayers on Au substrates obtained with Pt and Au tips was 0.79 and 0.72 nm respectively.

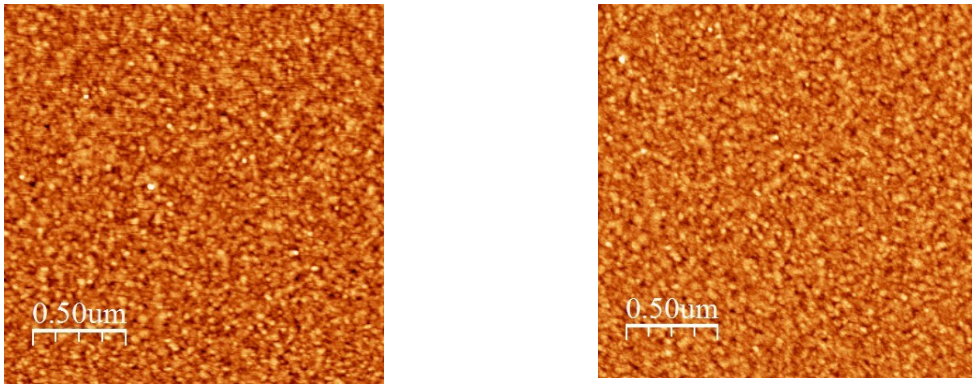

SI-10) Geometric modelling of gating has been done by van der Zant et al., who showed that a 2 nm molecule, sitting on a gate-oxide that is 10 to 100 nm thick, yields a gate coupling in the range 0.01 to 0.1 eV/V [3]. The gate-coupling value obtained from our configuration is lower, due to a lower dielectric constant of the gate and screening of the gate field. However, our method is empirical, aided by measurement of the work function of the electrodes as a reference, and can be evaluated at room temperature. This is in contrast with other methods used to quantitatively calculate the gate coupling in molecular electronics, such as single electron transistor (SET) measurements (normally carried out at cryogenic temperatures) where the gate-coupling values are calculated from the slope of coulomb diamonds on a conductance stability map [4].

For comparison, C. Cuevas and E. Scheer reported that (typically) a 250 nm SiO_2 gate oxide with 100 V_G range yields a ± 0.1 eV change in the potential of the molecule in a junction, i.e. a gate coupling of 10^{-3} eV/V_G [5]. In our setup an 80 nm gap in inert atmosphere with 20 V_G range yields 8 x 10^{-3} eV/V_G .

It should be noted that 50 % and 65% of the junctions in Pt-Azurin-Au and Au-Azurin-Au, respectively, did not show a gate effect. Sweeping the gate voltage, at a 10 mV_{SD} bias, did not show a change in the conductance even though two-terminal I_{SD}-V_{SD} currents were measured before and after the gate sweep with currents of the expected order of magnitude. As mentioned in the body of the text (in the section called 'reproducibility test'), there are many possible geometric pitfalls that preclude effective gate coupling. We assume that these lead, at times, to complete shielding of the gate field from the protein.

It was generally observed that there is a difference between the V_G onset in the forward sweep compared with the reverse sweep, as shown in fig. 2A of the main text. For the reader's convenience, we used the V_G onset for the forward sweep to make the calculation for the gate coupling. However, the *difference* between Pt and Au electrodes in the V_G onset (ΔV_G) for the forward and reverse sweep was similar: 6.6 $V_{G(forward)}$ and 6.3$V_{G(reverse)}$ respectively.

It is not possible to measure any possible lateral tip shift during the forward and backward V_G sweep. Therefore, we cannot exclude the possibility of drift, but as the results make this highly unlikely, we did not consider it further.

References

(1) Zaballa, M.-E.; Abriata, L. A.; Donaire, A.; Vila, A. J. Flexibility of the metal-binding region in apo-cupredoxins. *Proceedings of the National Academy of Sciences* **2012**, *109*, 9254-9259.

(2) Ruiz, M. P.; Aragonès, A. C.; Camarero, N.; Vilhena, J.; Ortega, M.; Zotti, L. A.; Pérez, R. n.; Cuevas, J. C.; Gorostiza, P.; Díez-Pérez, I. Bioengineering a single-protein junction. *Journal of the American Chemical Society* **2017**, *139*, 15337-15346.

(3) van der Zant, H. S.; Kervennic, Y.-V.; Poot, M.; O'Neill, K.; de Groot, Z.; Thijssen, J. M.; Heersche, H. B.; Stuhr-Hansen, N.; Bjørnholm, T.; Vanmaekelbergh, D. Molecular three-terminal devices: fabrication and measurements. *Faraday discussions* **2006**, *131*, 347-356.

(4) Perrin, M. L.; Burzurí, E.; van der Zant, H. S. Single-molecule transistors. *Chemical Society Reviews* **2015**, *44*, 902-919.

(5) Cuevas, J. C.; Scheer, E.: *Molecular electronics: an introduction to theory and experiment*; World Scientific, 2010.